Published in final edited form as:
J Microelectromech Syst. 2010 August ; 19(4): 743–751. doi:10.1109/JMEMS.2010.2050194.

A Microfluidic Device for Continuous-Flow Magnetically Controlled Capture and Isolation of Microparticles

Yao Zhou,
Department of Mechanical Engineering, Columbia University, New York, NY 10027 USA

Yi Wang, and
CFD Research Corporation, Huntsville, AL 35805 USA

Qiao Lin
Department of Mechanical Engineering, Columbia University, New York, NY 10027 USA

Qiao Lin: qlin@columbia.edu

Abstract

This paper presents a novel microfluidic device that exploits magnetic manipulation for integrated capture and isolation of microparticles in continuous flow. The device, which was fabricated from poly(dimethylsiloxane) (PDMS) by soft-lithography techniques, consists of an incubator and a separator integrated on a single chip. The incubator is based on a novel scheme termed target acquisition by repetitive traversal (TART), in which surface-functionalized magnetic beads repetitively traverse a sample to seek out and capture target particles. This is accomplished by a judicious combination of a serpentine microchannel geometry and a time-invariant magnetic field. Subsequently, in the separator, the captured target particles are isolated from nontarget particles via magnetically driven fractionation in the same magnetic field. Due to the TART incubation scheme that uses a corner-free serpentine channel, the device has no dead volume and allows minimization of undesired particle or magnetic-bead retention. Single-chip integration of the TART incubator with the magnetic-fractionation separator further allows automated continuous isolation and retrieval of specific microparticles in an integrated manner that is free of manual off-chip sample incubation, as often required by alternative approaches. Experiments are conducted to characterize the individual incubation and separation components, as well as the integrated device. The device is found to allow 90% of target particles in a sample to be captured and isolated and 99% of nontarget particles to be eliminated. With this high separation efficiency, along with excellent reliability and flexibility, the device is well suited to sorting, purification, enrichment, and detection of micro/nanoparticles and cells in lab-on-a-chip systems.

Index Terms

Cell sorting; magnetic manipulation; micro-fluidics; on-chip incubation; particle separation

I. Introduction

Microfluidic particle separation involves the capture, isolation, and collection of target particles from impure or complex samples and is widely used in sorting, purification, enrichment, and detection of cells [1]–[4] in cell biology, drug discovery, and clinical diagnostics. A number of methods currently exist for particle separation on microfluidic platforms, such as size-based separation [5]–[9], acoustic separation [10], dielectrophoresis

Color versions of one or more of the figures in this paper are available online at http://ieeexplore.ieee.org.

[11], [12], and fluorescence- [13], [14] and magnetic-activated separation [15], [16]. Among these, methods based on magnetic control are particularly attractive, which utilize surface-functionalized magnetic beads to capture target particles through specific binding and then to separate the target particles by magnetic manipulation. This separation scheme relies on the interaction of chemical bonds rather than geometrical or physical properties of the particles and hence allows highly specific and selective particle separation.

There are, in general, two operating modes for magnetically based microfluidic particle separation, i.e., batch mode and continuous flow mode. In the batch mode, target-bound magnetic beads are retained on a solid surface and subsequently released, following the removal of nontarget particles with a liquid phase. Magnetic bead beds [17] and sifts [18] have, for example, been developed for this purpose but have limited separation efficiency. A number of devices attempted to address this issue with various magnet designs, including a quadruple electromagnet [19], a planar electromagnet [20], nickel posts [21], etc. In addition, planar electromagnets can be integrated on chip with microvalves and micropumps to enable fully automated functionalities, such as fluid actuation and particle mixing [15]. Unfortunately, batch-mode designs suffer from several inherent limitations, including prolonged durations of operation, complicated fluidic handling, and, most importantly, significant contamination due to nonspecific trapping of impurities that are sequestered in the beads [22].

These limitations are effectively mitigated by continuous-flow magnetic particle separation, which typically employs magnetic fractionation, i.e., continuous accumulative deflection of magnetic beads. This method can be classified into two categories according to whether an integrated magnet or off-chip magnet is used. In the first category, magnetic microstrips, which are of typically alloy or ferromagnetic materials, are deposited on the device substrate to generate a magnetic field gradient that separates magnetic beads [23]–[25]. Substantial effort is required to design and fabricate on-chip magnetic strips, as well as fluidic components, to ensure balanced hydrodynamic and magnetic forces. Alternatively, in the second category, the use of a simple external magnetic setup in conjunction with on-chip separation enables great flexibility in device design and strong magnetic manipulation [16], [26]. Despite these notable features, existing magnetic separators are typically limited by prolonged off-chip incubation of target particles with magnetic beads, which is required to ensure sufficient bead-particle interaction and binding before on-chip separation. This is time consuming, labor intensive, and prone to contamination, and, in the case of cell separation, could potentially compromise the viability of target cells. Integration of an on-chip incubation module, in which target cells are captured by magnetic beads prior to separation, would effectively address this issue and is highly desired.

A suitable on-chip incubation technique is key to the on-chip incubation module. Due to low Reynolds flow and molecular diffusion-dominated transport mechanism inside the micrometer-sized channels, a variety of passive and active approaches have been investigated to enhance mixing in the incubation process [27]–[30]. Passive micromixers typically rely on diffusion or chaotic advection [31]–[33] and are inadequate for particle/bead incubation or prone to undesired bead retention/trapping at corner features. On the other hand, active mixers utilize flow agitation arising from an external field (e.g., an acoustic [34] or electrohydrodynamic [35], [36] field) to enhance mixing and typically require rather complicated fabrication and operation procedures.

This paper presents an integrated microfluidic device for automated continuous-flow magnetically controlled capture and isolation of target particles. A major innovation of the device lies in the use of a novel incubator that differs from traditional approaches requiring bulk fluid mixing and the integration of this incubator with a magnetic-fractionation-based

separator on a single chip. The incubator is based on the scheme of target acquisition by repetitive traversal (TART), in which surface-functionalized magnetic beads seek out and capture target particles by repetitively traversing the sample. This is accomplished by a judicious combination of a serpentine microchannel geometry and a time-invariant magnetic field. Using a simple corner-free serpentine-channel design without requiring bulk fluid mixing, the TART incubator has zero dead volume and minimizes undesired particle or magnetic-bead retention. With a planar design, the integrated device can be fabricated with a straightforward one-mask soft-lithography process and allows for fully automated operation with excellent separation efficiency and reliability. Thus, the device can be potentially of great utility for isolation and analysis of micro/nanoparticles and cells in lab-on-a-chip systems.

II. Principle and Design

In this section, we first elucidate the principle of the magnetically controlled capture and separation and then describe the device design and operating procedure.

The sample presented to the microfluidic device is a mixture of target microparticles, whose surfaces are functionalized with a biomolecule (or a ligand) and nontarget particles. These particles are a model of target and nontarget cells in a biological sample. In our approach, target particles are selectively isolated in a two-stage process. In the first stage, i.e., the *incubation stage*, the sample is incubated with magnetic beads, allowing target particles to be captured by specific ligand-receptor binding. That is, magnetic microbeads, whose surfaces are immobilized with a receptor molecule that specifically recognizes the ligand on the target particles, are introduced into the sample stream for binding under a magnetic field. Binding between the receptor and ligand leads to the complexation of target particles and magnetic beads. As a result, the target particles are captured by the magnetic beads. Next, in the second stage, i.e., the *separation stage*, the complexes of target particles and magnetic beads are separated from nontarget particles by magnetic fractionation under the same magnetic field as used for incubation, resulting in the isolation of target particles. For purposes of proof of concept, we use biotin as a ligand on the target particles and streptavidin as a receptor on the magnetic beads. As such, our method can readily be extended to manipulation of biological samples. For example, target cells can be captured and isolated using magnetic beads functionalized with receptor molecules specifically recognizing membrane proteins on the cells.

According to these two stages, the microfluidic device (Fig. 1) consists of two major components integrated on a single chip, i.e., an incubator in which the sample and magnetic beads are incubated for capture of target particles and a separator in which captured target particles are isolated from nontarget particles. While the separator is based on well-established magnetic fractionation principles, the incubator exploits a novel scheme termed TART, in which magnetic beads seek out and capture target particles by repetitive traversal through the sample by a judicious combination of geometry and magnetic force. The TART incubator and magnetic-fractionation separator are described here.

A. TART Incubator

In the TART incubation scheme, a sample and magnetic-bead suspension flow side by side in a two-stream configuration in a serpentine-shaped channel; magnetic beads repetitively traverse the sample stream to seek out and capture target particles. As shown in Fig. 1, the sample and magnetic-bead suspension are introduced through their respective inlets, merge at a Y-junction, and then enter the incubation channel, which is a serpentine microchannel consisting of a series of parallel straight channel sections connected by U-shaped turns and placed next to a bar-shaped permanent magnet. Low-Reynolds-number conditions allow the

sample and magnetic-bead suspension to flow side by side as two laminar streams throughout the incubation channel. In the absence of a magnetic field, target and nontarget particles, as well as magnetic beads, would also remain in their respective fluid streams with negligible lateral diffusion due to their relatively large sizes. With the lateral magnetic field generated by the permanent magnet in the straight channel sections, magnetic beads are pulled toward the magnet (i.e., to the left in Fig. 1). Thus, the beads, which are initially located in the right-side stream in the leftmost straight section of the incubation channel, deflect to the left and cross the flow streamlines. Immediately after passing the first U-turn, the magnetic beads follow the streamlines and emerge again on the right side when entering the next straight channel section. In the subsequent sections downstream, this process is repeated, with the beads alternately shuttled between left and right. This repetitive lateral traversal of magnetic beads in the sample stream allows the beads to effectively seek out and capture target particles. The use of a serpentine channel free of dead volume allows minimization of undesired particle or bead retention during incubation.

The magnetic pulling force experienced by magnetic beads in general varies with the distance of the straight channel sections from the permanent magnet. To address this practical issue and allow for consistent traversal of magnetic beads in the incubation channel sections, the incubator design employs straight channel sections whose widths are proportional to their distance from the permanent magnet. Given flow continuity, such a design allows reduced flow speeds and longer residence times in the channel sections at farther distances from the magnet to compensate for the weakened magnetic force therein. This effectively minimizes undesired particle retention in the upstream channel sections (which are relatively close to the magnet) and ensures adequate bead deflection in the downstream sections (which are relatively far away from the magnet).

B. Magnetic-Fractionation Separator

The bead-captured target particles emerge from the TART incubator and enter the separator, where they are isolated from the nontarget particles by magnetic fractionation (Fig. 1). The separator includes an additional inlet (termed the buffer inlet), which merges with the separator entrance to form a wide straight channel section. A stream of pure buffer (free of particles and beads) is introduced into the buffer inlet and combines with the mixture of bead-captured target particles and nontarget particles that has just exited the incubator. Note that the mixture may also include a small number of uncaptured target particles or unused magnetic beads; however, they do not interfere with the separation process and hence will be ignored in the following discussion. The buffer and mixture will form two side-by-side laminar streams in the separator channel. As they move downstream, the bead-bound target particles are driven toward the magnet, crossing the buffer stream and becoming separated from the nontarget particles that remain in the sample stream. Thus, two outlets at the end of the collection channels following the separator channel, which are termed the target and waste outlets, can be used to collect the bead-captured target particles and nontarget particles, respectively. As the flow rate of the sample at the separator entrance is considerably less than that of the buffer at the buffer inlet, the nontarget particles that remain in the sample stream will be constrained within a very thin layer near the right side wall of the separator channel and will completely exit via the waste outlet. Therefore, the bead-captured targets collected at the target outlet will be pure, i.e., free of nontarget particles. This effectively addresses the limited degree of purification in most batch-mode magnetic separation processes due to the false trapping of nontarget particles. In addition, the flow rates for the buffer and mixture streams are judiciously selected to produce an adequate hydrodynamic driving force and prevent magnetic beads from adhering to the channel walls.

III. Materials and Methods

The device consists of a sheet of poly(dimethylsiloxane) (PDMS) bonded to a glass slide. The microfluidic features were fabricated in the PDMS sheet using soft lithography techniques. Briefly, the fabrication process began with spin-coating and patterning of a 30-μm layer of SU-8 2025 photoresist (MicroChem, Newton, MA) on a silicon wafer, which, upon curing at 95 °C for 5 min on a hotplate, formed a master defining the negative of the desired microfluidic features. Next, a PDMS prepolymer (Sylgard 184, Dow Corning, Midland, MI) was cast against the master and cured at 70 °C for 35 min, also on the hotplate. The resulting PDMS sheet was then peeled off from the master, cut into suitably sized pieces, and punched with inlet and outlet holes. The PDMS was bonded to a glass slide after a 10-min treatment in an ultraviolet ozone cleaner (Model T10X10/OES, UVOCS, Lansdale, PA). Tygon tubes were inserted into the inlet and outlet holes in the PDMS to establish micro-to-macrofluidic interconnects. An image of a fabricated device is shown in Fig. 2(a), with ink solution filled in the channel to aid visualization. The dimensions of the TART incubator and separator are shown in Fig. 2(b) and (c), respectively.

Materials used in the experiments included 5% bovine serum albumin (BSA) (Sigma-Aldrich, St. Louis, MO), 2.8-μm streptavidin-coated magnetic beads, 0.4-μm biotin-coated green fluorescent polystyrene particles (as target particles), and 0.4-μm uncoated red fluorescent polystyrene particles (as nontarget particle) (all from Spherotech, Lake Forest, IL). The magnetic bead diameter was chosen based on a tradeoff between the needs for reducing sedimentation and ensuring sufficient magnetically driven migration mobility of the beads. The size of polystyrene particles represented those of various bacterial cells. Three samples were used in the experiments: 1) a suspension of streptavidin-coated magnetic beads (0.5% w/v) supplemented with BSA; 2) a mixture of biotin-coated particles (0.1% w/v) and uncoated particles (0.1% w/v) in suspension, supplemented with BSA (target versus nontarget ratio: 1 : 1); and 3) a mixture of biotin-coated particles (0.05% w/v) and uncoated particles (0.5% w/v) in suspension, supplemented with BSA (target versus nontarget ratio: 1 : 10). Deionized (DI) water was used as a running buffer supplied to the separator. Before the experiments, the microfluidic channels were incubated with 2% BSA solution for 2 h to block nonspecific adsorption and then flushed with DI water. Samples and buffer were driven into appropriate inlets of the device using syringe pumps (KD210P, KD Scientific, Holliston, MA, and NE-1000, New Era Pump Systems, Wantagh, NY). A 50-mm-long bar-shaped Neodymium permanent magnet (McMaster-Carr, Elmhurst, IL) was placed alongside the device. Bright field images of magnetic beads, as well as fluorescent images of target and nontarget fluorescent particles, were taken using an inverted epi-fluorescent microscope (Diaphot 300, Nikon Instruments, Melville, NY) and recorded by a charge-coupled-device camera (Model 190CU, Micrometrics, Londonderry, NH). Images were analyzed, and quantitative data were extracted using ImageJ (available free online at http://rsb.info.nih.gov/ij/). The concentration of magnetic beads and those of target and nontarget particles were determined by analyzing the intensity of bright field or fluorescent images as appropriate in three rectangular regions located at the Y-junction, the end of the incubator, and the end of the separator, respectively (Fig. 1). These regions were aligned with the channel and were of equal width to the channel and length 1 mm along the channel. The regions were each further divided into ten lanes of equal width to facilitate the calculation of magnetic bead and particle distributions across the channel.

IV. Results and Discussion

In this section, we first individually characterize the TART incubator and magnetic-fractionation separator at the component level by examining and comparing particle distributions across the channels at their exits. Then, the behavior of the integrated device is

investigated at multiple locations to demonstrate its capability of capture and isolation of target particles.

A. Incubator Characterization

We examined the efficiency of the TART scheme in the incubator. A permanent-magnet bar was placed to the immediate left of the device (Fig. 1). Magnetic beads were injected from the bead inlet, and a suspension of target and nontarget particles at 1 : 1 ratio was injected from the sample inlet, both at a flow rate of 0.5 μL/min, corresponding to an average velocity that varied from 5.6 to 2.8 mm/s along the incubator channel [Fig. 2(b)]. This flow rate was chosen as a tradeoff between the need to reduce the retention of magnetic beads on the channel wall and the need to ensure sufficient traversal time of magnetic beads in the sample.

Fig. 3 is a snapshot image of the trajectories of magnetic beads within the TART incubator. It clearly shows that, after passing each turn, magnetic beads laterally traverse the streamlines and move toward the left side of each straight channel section. This repetitive traversal of the sample by magnetic beads in the incubation channel markedly improves the contact probability and facilitates binding between the beads and the particles. Although a moderate number of magnetic beads could be retained at the turns during operation, the bead inflow and outflow at the turns will eventually reach equilibrium, and the number of beads retained remains insufficient to cause channel clogging. In addition, we observed in the experiments that the retained beads can easily be flushed away by increasing the flow rate and/or reducing the magnetic force at the end of the operation to minimize loss of beads.

The following analysis and experimental observation can be used to further assess the essential role of the TART scheme in enhancing target particle capture during incubation. First, there is a lack of lateral diffusion of sample particles and magnetic beads. As they traverse the entire length of the incubator channel at the aforementioned chosen flow rate, the characteristic lateral diffusion distance is estimated to be about 9 μm for the target particles and 2 μm for the magnetic beads. Compared with the incubator channel width (100–200 μm), these diffusion distances are clearly inadequate for the effective interaction of the target particles and magnetic beads. Second, the interactions of target particles and magnetic beads caused by the secondary flow in the turns of the incubator channel are negligible, as indicated by a very small Dean number [37], which is in the range of 0.06–0.12 when calculated using typical geometric and material properties. Due to the insignificance of diffusion and secondary flow, an active means of promoting the interaction of target particles and magnetic beads is necessary and is offered by the TART scheme.

In addition, we experimentally demonstrate the necessity of the TART scheme by comparing the distributions of target particles in the incubator with and without using the TART scheme. To facilitate this comparison, the observation was made at a position immediately preceding the last turn of the incubator (Fig. 4). When TART was used, most target particles interacted and bound to the magnetic beads and were hence pulled toward the left channel wall. This is seen in the concentrated distribution of target particles near the left channel wall [Fig. 4(a)]. On the other hand, in the absence of TART, the target particles and magnetic beads remained in their separate laminar streams, as reflected by the fluorescence signal being limited within the sample stream (located on the right-hand side of the channel [Fig. 4(b)]). The differences between observations with and without TART are also graphed in Fig. 4(c), which are clearly significant, and indicate that the TART scheme is essential to ensuring effective capture of target particles by magnetic beads.

Having demonstrated the importance of the TART scheme, we then quantitatively examined the incubator behavior with TART in terms of particle capture at the Y-junction of incubator

inlets and at the incubator exit and compared the differential effects of the magnetic force on the target and nontarget particles. Fluorescent images of target (green) and nontarget (red) particles at the Y-junction of the incubator are shown in Fig. 5 (panels a and b, respectively). The particle sample and magnetic-bead suspension formed two distinct side-by-side streams in the upper and lower halves of the Y-junction, respectively, with negligible mixing. Fig. 5(c) quantitatively depicts the distributions of target and nontarget particles at the Y-junction. It can be seen that the target and nontarget particles were both highly concentrated in lanes 1–5, containing over 95% of the target and nontarget particles, whereas, in lanes 6–10, the presence of the target and nontarget particles was negligible. This indicates that, at the Y-junction, the particles were not mixed with the magnetic beads.

Next, we investigated the particle distributions at the end of the incubator. The fluorescent images of target (green) and nontarget (red) at the end of the incubator are given in Fig. 6(a) and (b). It can be seen that the target particles captured by the magnetic beads in the serpentine channel were mostly attracted to the left, where the permanent magnet is placed. On the other hand, the free nontarget particles spread out and were quite uniformly distributed across the channel width, primarily due to flow agitation by magnetic beads in the serpentine incubation channel.

The quantitative particle distributions across the channel width at the end of the incubator are extracted and plotted in Fig. 6(c). The majority of target particles (95.9%) appeared on the left half of the channel, whereas the nontarget particles were evenly distributed across the channel width. The highest concentration of target particles did not occur in lane 1, which may be attributed to the slight magnetization of target-bound magnetic beads and their aggregation on the left channel wall. Upon magnetization, the target-bound magnetic beads tended to aggregate into an oval-shaped cloud with tens of micrometers in size that is a few times larger than the lane width (20 μm). Therefore, when the oval cloud was attracted to the left side of the channel, lane 1 could only probe the edge of the oval containing a small number of target particles, whereas the center of the oval fell in lane 2 and included more target particles. The aggregation of magnetic beads also accounted for the local discontinuity in the bead suspension stream as observed.

B. Separator Characterization

Next, we characterized the separator in terms of its capacity to deflect and extract magnetic beads. For the purposes of this study, we fabricated a chip that exclusively contained the separator. The permanent magnet was again placed to the left of the chip. A suspension of bare magnetic beads was introduced into separator entrance at a flow rate of 1 μL/min, whereas DI water was introduced into the buffer inlet at 4 μL/min. As shown in Fig. 7(a), when first entering the separation channel from the separator entrance, the beads were highly concentrated to the right side of the separator due to laminar flow behavior. At the exit, however, they were attracted toward the magnet and accumulate at the left-hand side [Fig. 7(b)].

We compared bead distributions across the channel width at the separator exit in the cases with or without the permanent magnet. An observation region at the separator exit was selected, where the channel width was again divided into ten lanes and the percentage of beads falling into each lane was obtained to quantify the bead distributions. As the target and waste collection channels (Fig. 1) have similar hydrodynamic resistances, beads (and particles) located in the five left lanes would exit via the target exit, whereas those in the five right lanes would exit from the waste exit. As shown in Fig. 7(c), the magnetic force caused the beads to concentrate to the left, with 90.3% located in lane 1 and 96.2% falling within lanes 1–5. On the other hand, without the magnetic field, the majority of beads remained in the right lanes, with 96.7% of them in lanes 6–10 and exiting from the right-side

waste exit [Fig. 7(c)]. These results substantiate that the deflection and separation of the magnetic beads from its original streams were indeed caused by the presence of the magnetic field.

C. Integrated Device Characterization

Having individually characterized the TART incubator and magnetic-fractionation separator, we then investigated a complete microfluidic device with both the incubator and the separator integrated on a single chip. With the same experimental setup, we injected a suspension of premixed target and nontarget particles into the device's incubator via the sample inlet and a suspension of magnetic beads via the bead inlet, each at a flow rate of 0.5 μL/min. The particle suspension sample was prepared at two ratios of target to nontarget particle concentrations (1 : 1 and 1 : 10). DI water was infused via the buffer inlet into the separator at a flow rate of 4 μL/min. We examined particle distributions at the end of the separator to examine the ability of the integrated device to capture and isolate target particles.

Fig. 8(a) and (b) presents fluorescence images of target and nontarget particles, from a sample of 1 : 1 target-to-nontarget ratio, which was taken within the separator observation region (Fig. 1) immediately upstream the separator exits. It can be seen that the target and nontarget particles were clearly separated at the left and right sides of the channel with negligible overlap. Distributions of the particles are extracted from the experimental data and plotted in Fig. 8(c). We can observe that the majority of the target particles (bound with magnetic beads) were attracted to the left side of the channel, with 87.0% of them contained in lane 1, whereas the nontarget particles remained in lanes 9 and 10. Overall, 92.7% of target particles were retrieved at the target outlet (corresponding to lanes 1–5), whereas 99.9% of the nontarget particles were collected at the waste outlet.

The crucial role of the TART scheme in target capture was also investigated with this integrated device (further supporting observations made in Section IV-A). To this end, we examined the distributions of target particles at the end of the separator following incubation with and without TART. When TART was enabled, target particles were successfully captured by magnetic beads and then deflected by magnetic force to the left of the separator, as shown in Fig. 8(a), which is duplicated in Fig. 9(a) for purposes of comparison. In the case of incubation without TART, target particles largely remained free from magnetic beads and stayed on the right side of the separator. The dashed line (in white) superimposed on the images indicates the interface between the streams entering the separator from the buffer inlet and incubator exit (Fig. 1). Note that the latter stream further consisted of two streams introduced into the incubator from the sample and bead inlets, respectively (Fig. 1). These two streams had become well mixed in the incubator due to agitation by TART-enabled magnetic bead migration [Fig. 9(a)] but remained well separated by a clearly visible interface when TART was disabled [Fig. 9(b)]. The fluorescent images can also be used to obtain particle percentage distributions across the separator channel width [Fig. 9(c)]: 87% of target particles were located in lane 1 with TART enabled, whereas 71% of target particles remained in lanes 9 and 10 with TART disabled. These results demonstrate that the capture and separation of target particles were successful with TART and failed in the absence of TART.

Separation results with TART enabled obtained from another sample with a 1 : 10 ratio of target to nontarget particle concentrations were qualitatively the same (Fig. 10), except that lower fluorescent intensities were obtained due to the lower relative concentration of target particles in the sample with respect to nontarget particles. Specifically, 88.0% of the target particles were obtained in lane 1. Overall, 91.1% and 99.3% of the target and nontarget particles were collected at their respective outlets, respectively.

In general, the target capture and separation efficiency increases with the concentration of magnetic beads and approaches 100% at sufficiently high bead concentrations. The efficiency observed in our experiment (92.7% and 91.1% for the 1 : 1 and 1 : 10 target versus nontarget ratios, respectively) favorably compares with other magnetically controlled particle separation devices incorporating different (e.g., diffusion-based) on-chip incubation schemes (e.g., the device of [31], in which target particles retrieved at the outlet are still contaminated with a significant concentration of nontarget particles). The capture and separation efficiency would further be improved with a higher magnetic bead concentration, which is however associated with an increased tendency of excessive bead retention and channel clogging.

V. Conclusion

A novel integrated microdevice for specific capture and separation of target microparticles using magnetic manipulation in continuous flow has been presented. The device utilizes surface-functionalized magnetic beads as a vehicle of magnetic manipulation, which allows specific capture of target particles by ligand-receptor binding and separation of target from non-target particles. Comprised of an incubator and a separator connected in series, the device exploits the synergetic effects of laminar hydrodynamic flow and magnetic force to achieve target particle capture and fractionation. In contrast to existing particle separation devices, this approach offers simplicity in device fabrication and operation and can potentially allow cell assays to be rapidly performed with high specificity and selectivity.

With judiciously selected geometrical parameters, the device was fabricated using soft-lithography techniques. Experiments were conducted to characterize the incubator and separator at the component level, as well as on the integrated device. Experimental results have demonstrated that the device is capable of specifically capturing, isolating, and extracting target particles in a highly efficient continuous manner. Several key insights can be gained through the presented research effort, including the following:

First, the incubation module is based on the scheme of TART of surface-functionalized magnetic beads. By a judicious combination of a serpentine microchannel geometry and a time-invariant magnetic field, magnetic beads seek out and capture target particles by repetitively traversing the sample. Using a simple corner-free serpentine-channel design and without requiring bulk fluid mixing, the incubator is free of dead volume and minimizes undesired particle or magnetic-bead retention. Experimental results showed that, at the end of the incubation channel, the majority of target particles (95.9%) were captured by magnetic beads.

Second, the separation module capitalizes on the magnetic fractionation. Under the same magnetic field, magnetic beads were laterally deflected into a pure buffer stream and exited from the target exit. Experimental results have demonstrated that 90.3% of the magnetic beads were concentrated within the leftmost lane (lane 1) in the separator channel. In addition, 96.2% of all magnetic beads were located within the left half of the channel and extracted from the target outlet.

Finally, the integrated device incorporating both the incubator and separator has been tested using samples with two different ratios of target to nontarget particle concentrations (1 : 1 and 1 : 10). In both cases, more than 90% of target particles in the sample were captured, isolated, and extracted at the target outlet of the device. Meanwhile, more than 99% of nontarget particles in the sample were retrieved at the device’s waste outlet, confirming that the extraction obtained at the target outlet was practically free of nontarget particles.

These results demonstrate that the device is capable of capturing and isolating target particles from impure samples in an automated manner, with excellent separation efficiency and reliability. Thus, the device can potentially be useful for purification and analysis of biological micro/nanoparticles, such as bacteria and cells, in lab-on-a-chip systems.

Acknowledgments

This work was supported in part by the National Science Foundation under Grant CCR-0325344, Grant DBI-0650020, and Grant CBET 0854030, and in part by the National Institutes of Health under Grant RR025816-01A1. Subject Editor A. J. Ricco.

References

1. Chabert M, Viovy JL. Microfluidic high-throughput encapsulation and hydrodynamic self-sorting of single cells. Proc Nat Acad Sci USA. Mar; 2008 105(9):3191–3196. [PubMed: 18316742]
2. Lien KY, Lee WC, Lei HY, Lee GB. Integrated reverse transcription polymerase chain reaction systems for virus detection. Biosens Bioelectron. Mar; 2007 22(8):1739–1748. [PubMed: 16978853]
3. Murthy SK, Sethu P, Vunjak-Novakovic G, Toner M, Radisic M. Size-based microfluidic enrichment of neonatal rat cardiac cell populations. Biomed Microdevices. Sep; 2006 8(3):231–237. [PubMed: 16732418]
4. Zheng T, Yu HM, Alexander CM, Beebe DJ, Smith LM. Lectin-modified microchannels for mammalian cell capture and purification. Biomed Microdevices. Aug; 2007 9(4):611–617. [PubMed: 17516171]
5. Chen X, Cui DF, Liu CC, Li H, Chen J. Continuous flow microfluidic device for cell separation, cell lysis and DNA purification. Anal Chim Acta. Feb; 2007 584(2):237–243. [PubMed: 17386610]
6. Chmela E, Tijssen R, Blom M, Gardeniers H, van den Berg A. A chip system for size separation of macromolecules and particles by hydrodynamic chromatography. Anal Chem. Jul; 2002 74(14): 3470–3475. [PubMed: 12139056]
7. Huang LR, Cox EC, Austin RH, Sturm JC. Continuous particle separation through deterministic lateral displacement. Science. May; 2004 304(5673):987–990. [PubMed: 15143275]
8. Jain A, Posner JD. Particle dispersion and separation resolution of pinched flow fractionation. Anal Chem. Mar; 2008 80(5):1641–1648. [PubMed: 18220368]
9. Yamada M, Kano K, Tsuda Y, Kobayashi J, Yamato M, Seki M, Okano T. Microfluidic devices for size-dependent separation of liver cells. Biomed Microdevices. Oct; 2007 9(5):637–645. [PubMed: 17530413]
10. Petersson F, Nilsson A, Holm C, Jonsson H, Laurell T. Continuous separation of lipid particles from erythrocytes by means of laminar flow and acoustic standing wave forces. Lab Chip. Jan; 2005 5(1):20–22. [PubMed: 15616735]
11. Hu XY, Bessette PH, Qian JR, Meinhart CD, Daugherty PS, Soh HT. Marker-specific sorting of rare cells using dielectrophoresis. Proc Nat Acad Sci USA. Nov; 2005 102(44):15 757–15 761. [PubMed: 15615850]
12. Huang Y, Joo S, Duhon M, Heller M, Wallace B, Xu X. Dielectrophoretic cell separation and gene expression profiling on microelectronic chip arrays. Anal Chem. Jul; 2002 74(14):3362–3371. [PubMed: 12139041]
13. Fu AY, Chou HP, Spence C, Arnold FH, Quake SR. An integrated microfabricated cell sorter. Anal Chem. 2002; 74:2451–2457. [PubMed: 12069222]
14. Wang MM, Tu E, Raymond DE, Yang JM, Zhang HC, Hagen N, Dees B, Mercer EM, Forster AH, Kariv I, Marchand PJ, Butler WF. Microfluidic sorting of mammalian cells by optical force switching. Nat Biotechnol. Jan; 2005 23(1):83–87. [PubMed: 15608628]
15. Lien KY, Lin JL, Liu CY, Lei HY, Lee GB. Purification and enrichment of virus samples utilizing magnetic beads on a microfluidic system. Lab Chip. Jul; 2007 7(7):868–875. [PubMed: 17594006]
16. Pamme N, Wilhelm C. Continuous sorting of magnetic cells via on-chip free-flow magnetophoresis. Lab Chip. Aug; 2006 6(8):974–980. [PubMed: 16874365]

17. Furdui VI, Harrison DJ. Immunomagnetic T cell capture from blood for PCR analysis using microfluidic systems. Lab Chip. Dec; 2004 4(6):614–618. [PubMed: 15570374]
18. Earhart CM, Wilson RJ, White RL, Pourmand N, Wang SX. Microfabricated magnetic sifter for high-throughput and high-gradient magnetic separation. J Magn Magn Mater. May; 2009 321(10): 1436–1439. [PubMed: 20161248]
19. Ahn CH, Allen MG, Trimmer W, Jun YN, Erramilli S. A fully integrated micromachined magnetic particle separator. J Microelectromech Syst. Sep; 1996 5(3):151–158.
20. Choi JW, Oh KW, Thomas JH, Heineman WR, Halsall HB, Nevin JH, Helmicki AJ, Henderson HT, Ahn CH. An integrated microfluidic biochemical detection system for protein analysis with magnetic bead-based sampling capabilities. Lab Chip. Feb; 2002 2(1):27–30. [PubMed: 15100857]
21. Deng T, Prentiss M, Whitesides GM. Fabrication of magnetic microfiltration systems using soft lithography. Appl Phys Lett. Jan; 2002 80(3):461–463.
22. Recktenwald, D.; Radbruch, A., editors. Cell Separation Methods and Applications. New York: Marcel Dekker; 1998.
23. Berger M, Castelino J, Huang R, Shah M, Austin RH. Design of a microfabricated magnetic cell separator. Electrophoresis. Oct; 2001 22(18):3883–3892. [PubMed: 11700717]
24. Inglis DW, Riehn R, Austin RH, Sturm JC. Continuous microfluidic immunomagnetic cell separation. Appl Phys Lett. 2004; 85(21):5093–5095.
25. Adams JD, Kim U, Soh HT. Multitarget magnetic activated cell sorter. Proc Nat Acad Sci USA. Nov; 2008 105(47):18 165–18 170.
26. Espy MA, Sandin H, Carr C, Hanson CJ, Ward MD, Kraus RH. An instrument for sorting of magnetic microparticles in a magnetic field gradient. Cytometry A. Nov; 2006 69(11):1132–1142. [PubMed: 17051580]
27. Chang CC, Yang RJ. Electrokinetic mixing in microfluidic systems. Microfluid Nanofluid. Oct; 2007 3(5):501–525.
28. Hessel V, Lowe H, Schonfeld F. Micromixers—A review on passive and active mixing principles. Chem Eng Sci. Apr-May;2005 60(8/9):2479–2501.
29. Liu RH, Stremler MA, Sharp KV, Olsen MG, Santiago JG, Adrian RJ, Aref H, Beebe DJ. Passive mixing in a three-dimensional serpentine microchannel. J Microelectromech Syst. Jun; 2000 9(2): 190–197.
30. Nguyen NT, Wu ZG. Micromixers—A review. J Micromech Microeng. Feb; 2005 15(2):R1–R16.
31. Estes MD, Do J, Ahn CH. On chip cell separator using magnetic bead-based enrichment and depletion of various surface markers. Biomed Microdevices. Apr; 2009 11(2):509–515. [PubMed: 19082734]
32. Lund-Olesen T, Dufva M, Hansen MF. Capture of DNA in microfluidic channel using magnetic beads: Increasing capture efficiency with integrated microfluidic mixer. J Magn Magn Mater. Apr; 2007 311(1):396–400.
33. Stroock AD, Dertinger SKW, Ajdari A, Mezic I, Stone HA, Whitesides GM. Chaotic mixer for microchannels. Science. Jan; 2002 295(5555):647–651. [PubMed: 11809963]
34. Yang Z, Goto H, Matsumoto M, Maeda R. Active micromixer for microfluidic systems using Lead-Zirconate-Titanate (Pzt)-generated ultrasonic vibration. Electrophoresis. Jan; 2000 21(1): 116–119. [PubMed: 10634477]
35. El Moctar AO, Aubry N, Batton J. Electro-hydrodynamic microfluidic mixer. Lab Chip. Nov; 2003 3(4):273–280. [PubMed: 15007458]
36. Lin JL, Lee KH, Lee GB. Active micro-mixers utilizing a gradient zeta potential induced by inclined buried shielding electrodes. J Micromech Microeng. Mar; 2006 16(4):757–768.
37. Wang Y, Lin Q, Mukherjee T. Composable behavioral models and schematic-based simulation of electrokinetic lab-on-a-chip systems. IEEE Trans Comput-Aided Design Integr Circuits Syst. Feb; 2006 25(2):258–273.

Biographies

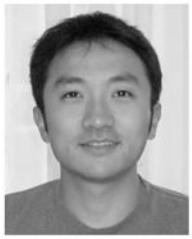

Yao Zhou received the B.S. degree in mechanical engineering and automation from Tsinghua University, Beijing, China, in 2003, and the M.S. degree in manufacturing engineering from Worcester Polytechnic Institute, Worcester, MA, in 2006. He is currently working toward the Ph.D. degree in mechanical engineering at Columbia University, New York, NY.

His research interests include designing microfluidic systems for biomedical applications, particularly cell manipulation and interrogation.

Yi Wang received the B.S. and M.S. degrees in mechanical engineering from Shanghai Jiao Tong University, Shanghai, China, in 1998 and 2001, respectively, and the Ph.D. degree in mechanical engineering from Carnegie Mellon University, Pittsburgh, PA, in 2005.

He is currently the Group Leader of the Micro and Nano Biosystems Group, CFD Research Corporation, Huntsville, AL. His research interests include development of microfluidic computational tools and design of microfluidic lab-on-a-chip systems for biomedical, life-science, and defense applications, in particular, highly integrated microelectrokinetic and nanoelectrokinetic devices.

Qiao Lin received the Ph.D. degree in mechanical engineering from the California Institute of Technology, Pasadena, in 1998, with thesis research in robotics.

From 1998 to 2000, he conducted postdoctoral research in microelectromechanical systems (MEMS) at the Caltech Micromachining Laboratory. From 2000 to 2005, he was an Assistant Professor of mechanical engineering at Carnegie Mellon University, Pittsburgh, PA. Since 2005, he has been an Associate Professor of mechanical engineering at Columbia

University, New York, NY. His research interests include designing and creating integrated microsystems/nanosystems, particularly MEMS and microfluidic systems, for biomedical applications.

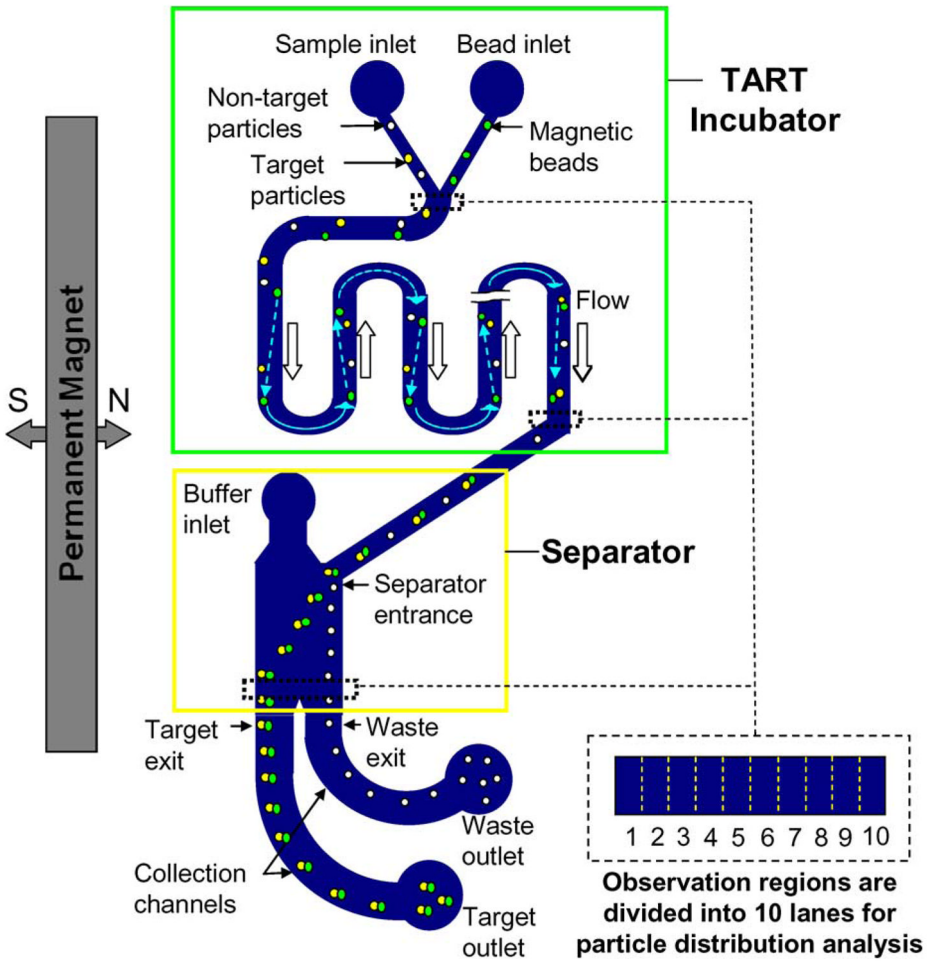

Fig. 1.

Schematic design of the microfluidic device for continuous-flow magnetically controlled capture and separation of microparticles. The device consists of an incubator that employs TART of magnetic beads and a separator that uses magnetic fractionation. The incubation and separator are serially connected and placed next to a bar-shaped permanent magnet. Particle distributions are analyzed in the observation regions at the Y-junction, the end of the incubator, and the end of the separator. These regions are each divided into ten lanes to facilitate the analysis.

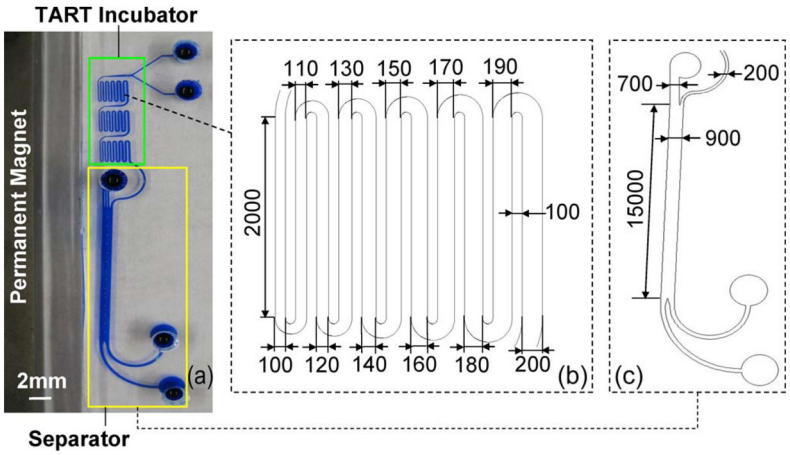

Fig. 2.

(a) Fabricated device (visualized with an ink solution). (b) Critical channel dimensions (in micrometers) of the TART incubator. (c) Critical channel dimensions (in micrometers) of the separator. (The channel depth is 30 μm for both the incubator and the separator.)

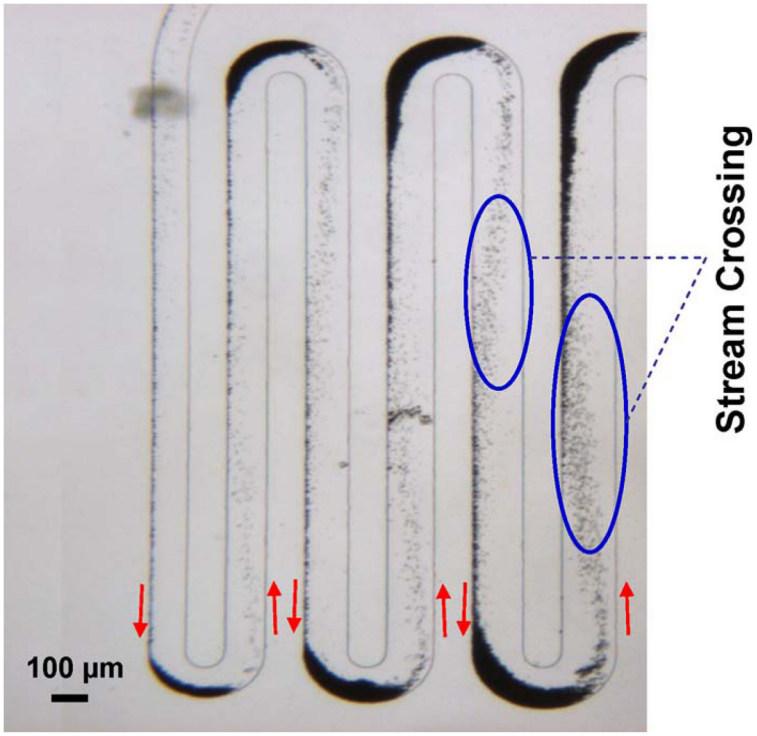

Fig. 3.
Micrograph image of magnetic microbeads migrating in the TART incubator.

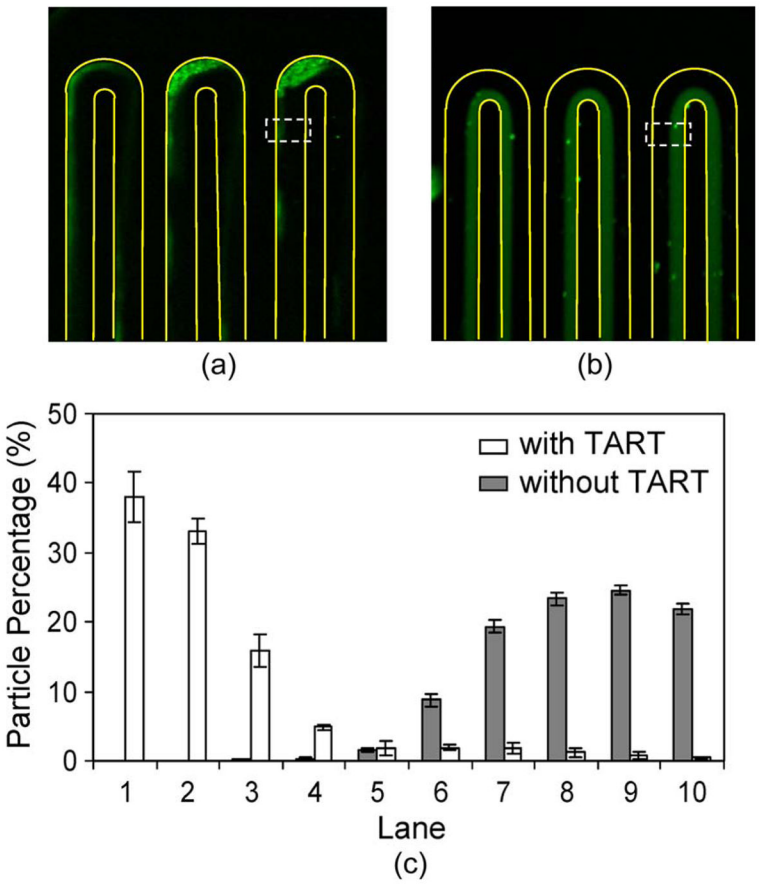

Fig. 4.

Comparison of incubation with and without using the TART scheme. (a) Fluorescent image of target particles with TART enabled. (b) Fluorescent image of target particles with TART disabled. (c) Percentage distributions of target particles across the channel width, in the dashed observation windows immediately preceding the last turn, as shown in the fluorescent images.

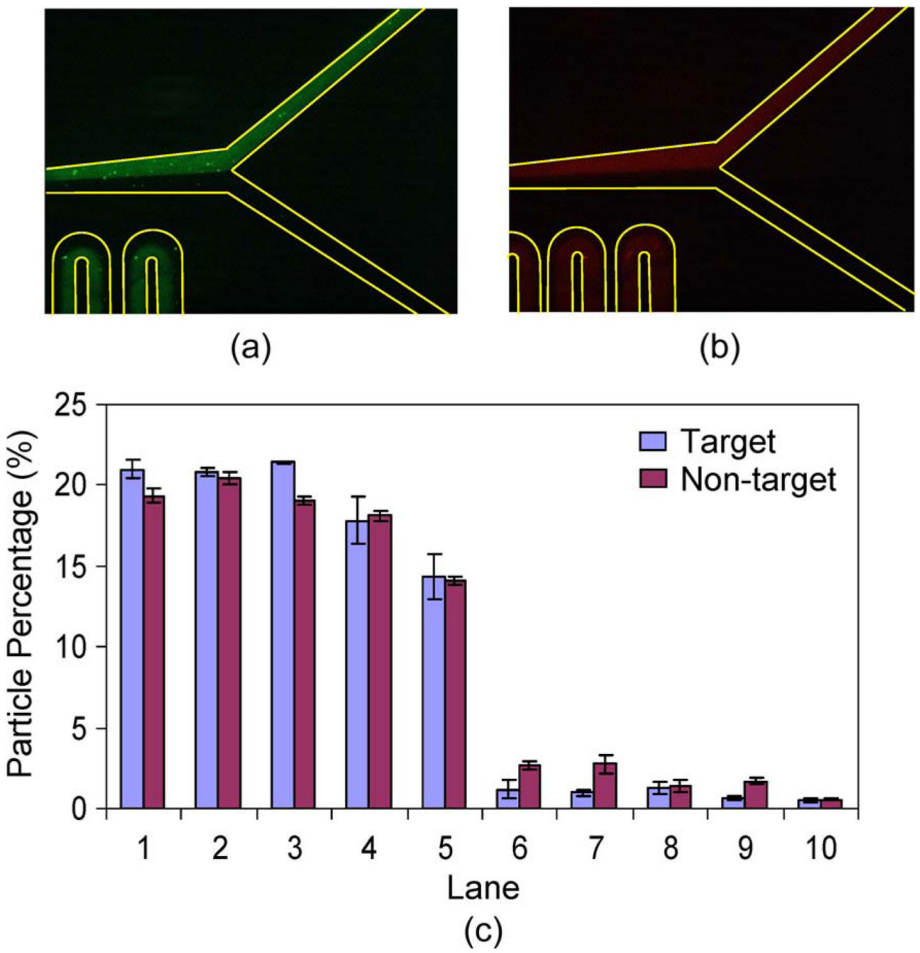

Fig. 5.

Distribution of target and nontarget particles across the channel width at the Y-junction. Fluorescent micrographs of (a) target particles and (b) nontarget particles at the Y-junction. (c) Percentage distributions of target and nontarget particles across the channel width at the Y-junction.

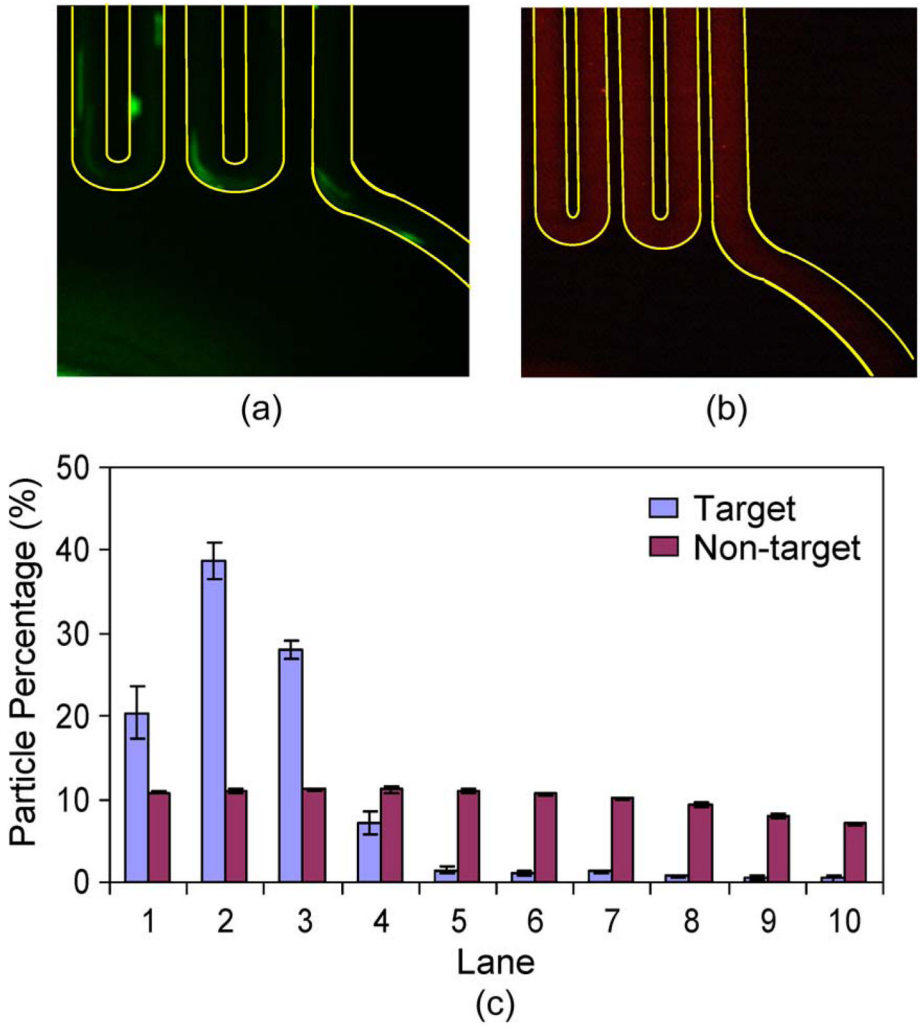

Fig. 6.

Distributions of target and nontarget particles across the channel width at the end of the TART incubator. A permanent magnet was placed to the left of the incubator channel. (a) and (b) Fluorescent micrographs of target and nontarget particles, respectively, at the end of the incubator. (c) Percentage distributions of target and nontarget particles across the channel width at the end of the incubator.

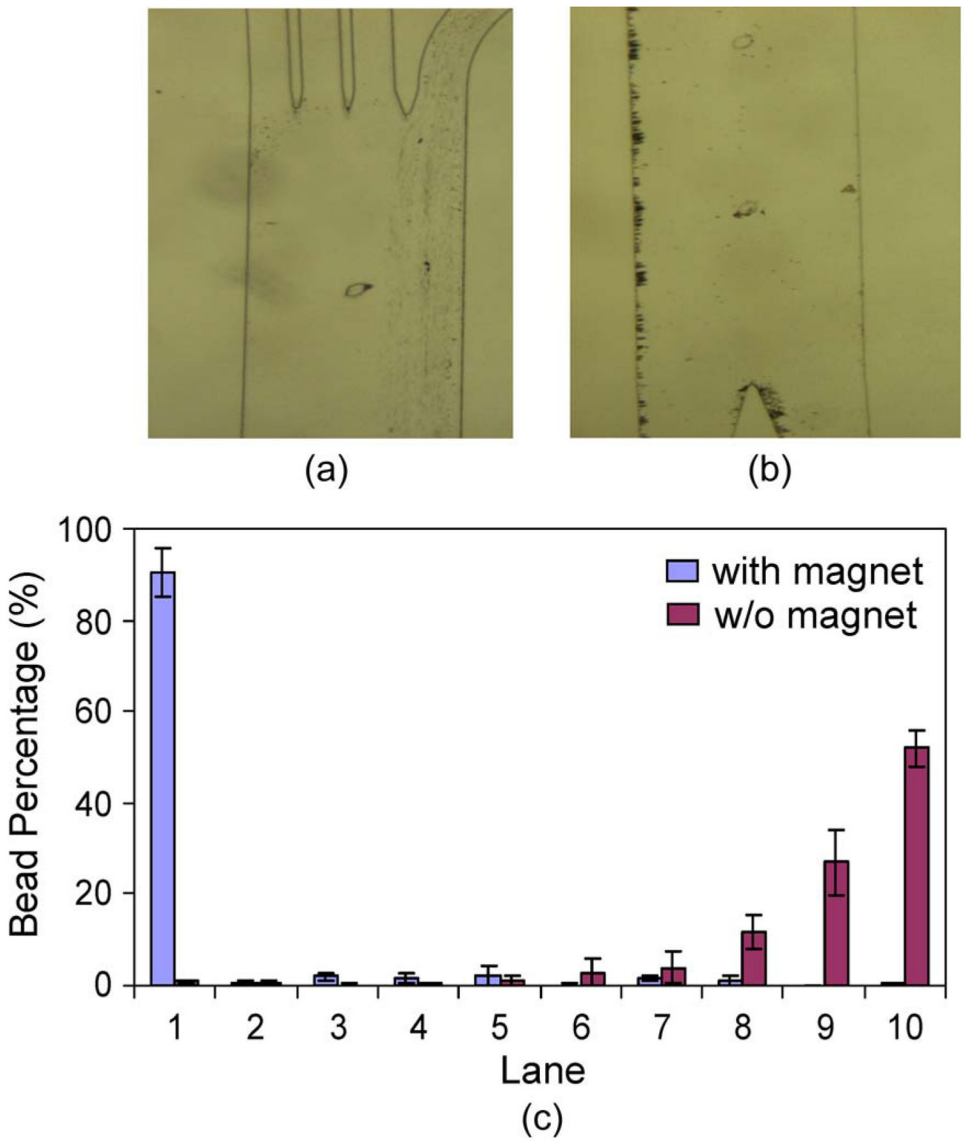

Fig. 7.

Characterization of particle separation within the separator using bare magnetic beads. (a) Image taken at the separator inlet. Magnetic beads entered the separator from the right. (b) Image taken at the separator exit. (c) Percentage distributions of magnetic beads at the separator exit.

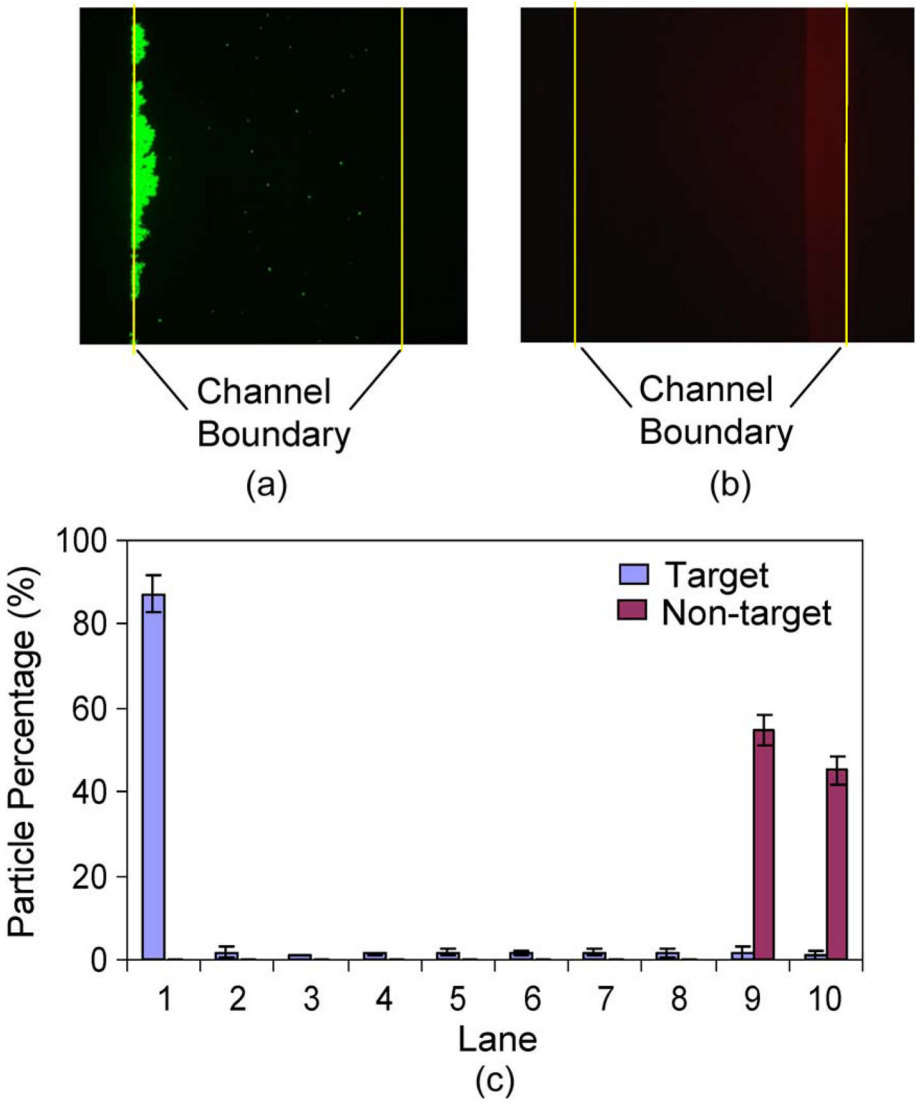

Fig. 8.

Distributions of target and nontarget particles across the channel width at the exit of the separator with a 1 : 1 ratio of target to nontarget particle concentrations, with the channel boundaries marked with yellow lines. (a) Fluorescent image of target particles. (b) Fluorescent image of nontarget particles. (c) Distributions of the target and nontarget particles across the channel width.

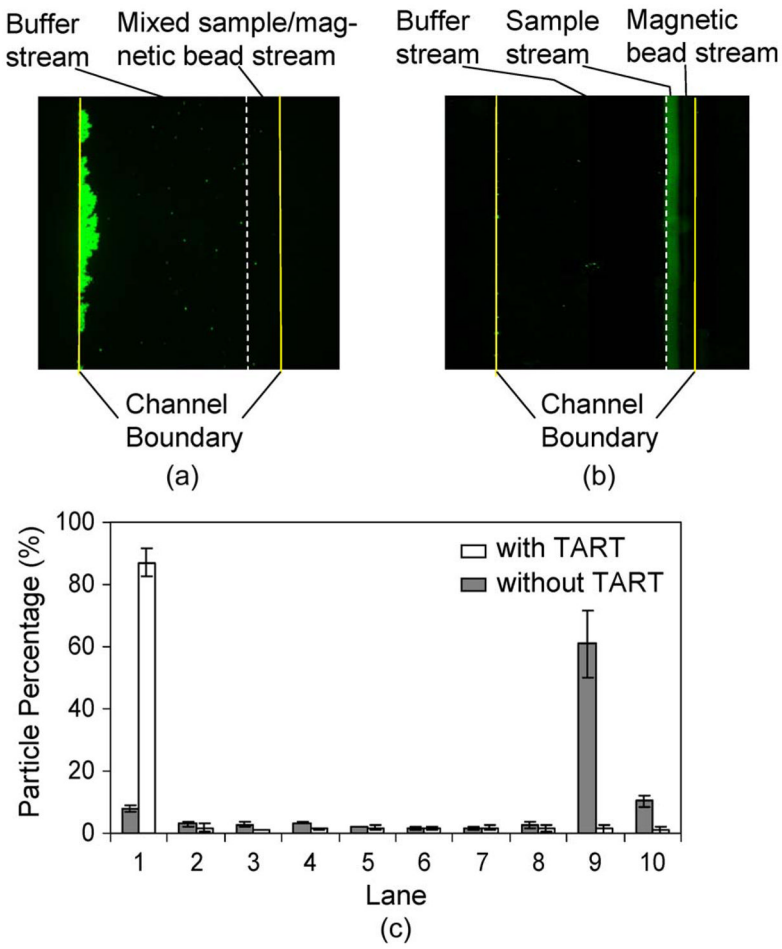

Fig. 9.

Comparison of separation with and without using the TART scheme. (a) Fluorescent image of target particles with TART enabled. (b) Fluorescent image of target particles with TART disabled. (c) Percentage distributions of target particles across the channel width at the end of the separator.

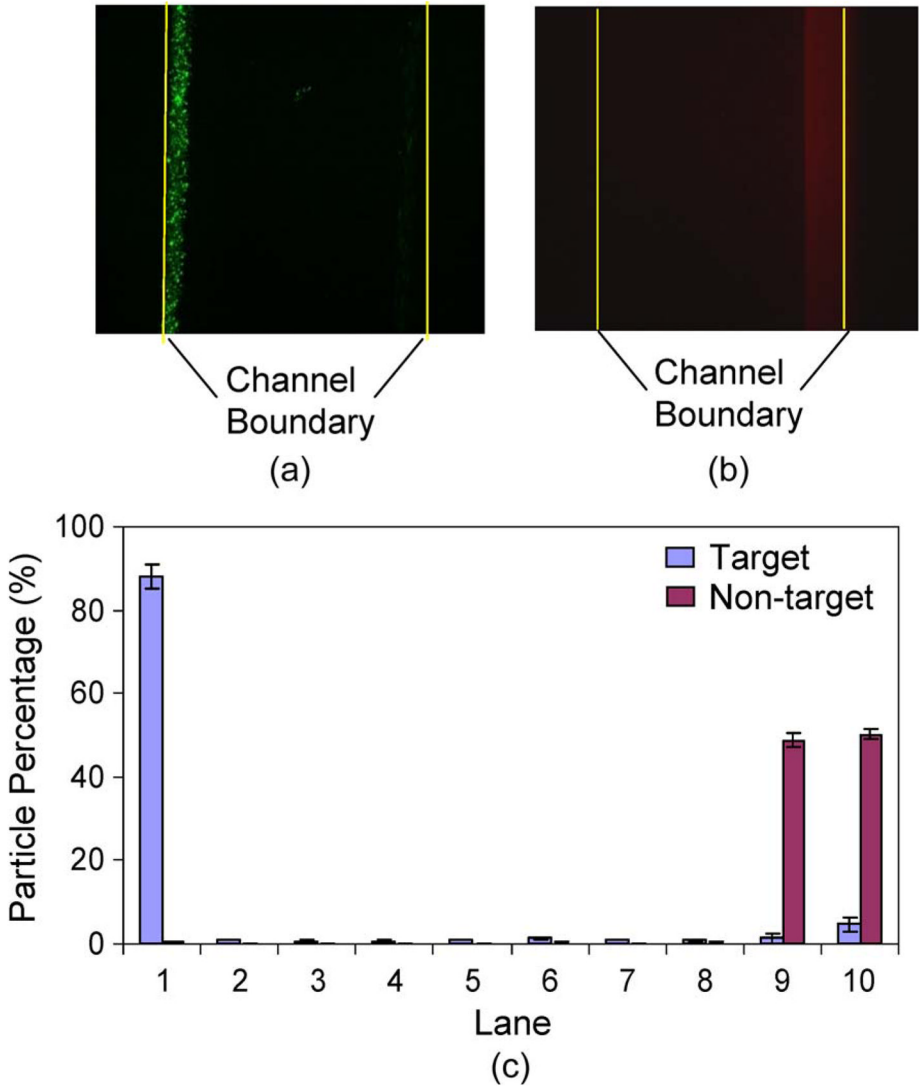

Fig. 10.

Distributions of target and nontarget particles across channel width at the exit of the separator with a 1 : 10 ratio of target to nontarget particle concentrations, with the channel boundaries marked with yellow lines. (a) Fluorescent image of target particles. (b) Fluorescent image of nontarget particles. (c) Distribution of target and nontarget particles in transverse lanes across the channel width.